Design of AlGaN/AlN Dot-in-a-Wire Heterostructures for Electron-Pumped UV Emitters

Ioanna Dimkou, Anjali A Harikumar, Akhil Ajay, Fabrice Donatini, Edith Bellet-Amalric, Adeline Grenier, Martien den Hertog, Stephen T Purcell, Eva Monroy

Design of AlGaN/AlN dot-in-a-wire heterostructures for electron-pumped UV emitters

*Ioanna Dimkou, Anjali Harikumar, Akhil Ajay, Fabrice Donatini, Edith Bellet-Amalric, Adeline Grenier, Martien I. den Hertog, Stephen T. Purcell, and Eva Monroy**

I. Dimkou, Dr. A. Grenier
Univ. Grenoble-Alpes, CEA-Leti, 17 av. des Martyrs, 38000 Grenoble, France

A. Harikumar, Dr. A. Ajay, Dr. E. Bellet-Amalric, Dr. E. Monroy
Univ. Grenoble-Alpes, CEA-IRIG-DEPHY-PHELIQS, 17 av. des Martyrs, 38000 Grenoble, France
E-mail: eva.monroy@cea.fr

Dr. F. Donatini, Dr. M. I. den Hertog
Univ. Grenoble-Alpes, CNRS-Institut Néel, 25 av. des Martyrs, 38000 Grenoble, France

Dr. S. T. Purcell
Univ. Lyon, Université Claude Bernard Lyon 1, CNRS, Institut Lumière Matière, 69622 Lyon, France

Keywords: ultraviolet, nanowires, AlGaN, quantum dot, lamp

This paper describes the fabrication of nitrogen-polar $Al_xGa_{1-x}N$/AlN (x = 0, 0.1) quantum dot superlattices integrated along GaN nanowires for application in electron-pumped UV sources. The nanowires are grown using plasma-assisted molecular-beam epitaxy on n-type Si(111) wafers using a low-temperature AlN nucleation layer. Growth conditions are tuned to obtain a high density of non-coalesced nanowires. To improve the uniformity of the height along the substrate, the growth begins with a base long nanowire (~900 nm), with a diameter of 30-50 nm. The $Al_xGa_{1-x}N$/AlN active region is 400 nm long (88 periods of quantum dots), long enough to collect the electron-hole pairs generated by an electron beam with an acceleration voltage ≤ 5 kV. The spectral response is tuned in the 340 to 258 nm range by varying the dot/barrier

thickness ratio and the Al content in the dots. Internal quantum efficiencies as high as 63% are demonstrated.

1. Introduction

UV light emitting diodes (LEDs) are in demand for disinfection purposes [1] at specific wavelengths. They also offer lower power consumption, the potential for longer lifetime, lower voltage requirement and non-toxic waste after use, as opposed to their mercury lamp counterparts. AlGaN is the material of choice for this technology because of its direct bandgap and the possibility to dope it both n-type and p-type [2,3]. Having said that, such devices have not reached their industrial maturity yet due to drawbacks in terms of electrical injection and light extraction, which limit their wall-plug efficiency (WPE) [4]. Let us remind that the *WPE* is the ratio between the optical output power and the electrical input power. WPE can be written as WPE = LEE × IQE × EIE, where LEE is the light extraction efficiency, IQE is the internal quantum efficiency (number of photons generated per electron-hole pair injected in the active medium), and EIE is the electron injection efficiency.

A promising alternative for the fabrication of highly efficient, eco-friendly UV lamps is based on the injection of electrons into AlGaN/AlN nanostructures using a miniaturized electron gun, e.g. a carbon nanotube cathode. An electron-pumped device looks like a vacuum tube or valve [5], which can be scaled down to millimeter size. Such a configuration avoids the problems associated with the carrier injection (dopant ionization energy, asymmetric carrier mobility of electrons and holes, realization of ohmic contacts). In the case of pumping with an electron beam, the average energy required to generate an electron-hole pair in a given semiconductor is close to 3 times its band gap energy [6]. Therefore, the electron injection efficiency is wavelength independent (EIE ≈ 1/3), and it should be possible to fabricate lamps operating close to the AlN band gap (e.g. 210 nm) if the IQE and LEE of the emitting structure is high enough. . In the spectral range generally used for disinfection, implantation of such a technology would depend basically on the cost per milliwatt of optical power, which could

become comparable to LEDs thanks to the higher device output power (easily scalable with the semiconductor surface) and simpler material growth and processing.

Electron-pumped emission from GaN and AlGaN quantum wells has been reported [7–12], but such lamps displayed low wall plug efficiency mostly due to the poor light extraction efficiency. Furthermore, stimulated emission around 350 nm has been demonstrated in electron-pumped GaN/AlGaN ridge structures under pulsed pumping [12–14]. For the implementation of such electron-pumped UV sources, the semiconductor geometry and conductivity must be adapted to maximize the energy conversion, light extraction and charge evacuation. There are several motivations to consider nanowires (NWs) for this application. First, their as-grown shape spontaneously favors light extraction [15], without additional processing requirements. In addition, the relatively easy implementation of three dimensionally confined objects (dots in a wire) results in high values of internal quantum efficiency (IQE) at room temperature [16]. Last but not the least, their direct growth self-assembled on silicon substrates reduces the cost of the system.

One of the main challenges for the growth of NW ensembles for electron-pumped UV sources is the homogeneity of the dot thickness and composition along an active region that is hundreds-of-nm long. It is known that the luminescence from GaN/AlGaN and AlGaN/AlN superlattices (SLs) on GaN NWs presents strong spectral dispersion, with broad and sometimes multi-line spectral profiles [17,18]. Such dispersion is due the variation of the dot height and diameter along the growth axis [19–21], the different strain relaxation in the dots along the growth axis [19,20,22], the presence of monolayer thickness fluctuations in the dots [19], and the alloy inhomogeneities and inter-diffusion phenomena at the hetero-interfaces, which depend on the strain state of the structure [18]. Additional perturbations can be introduced by coalesced areas and lateral GaN inclusions [23]. It is hence highly important to develop precisely controlled growth processes that allow the synthesis of homogeneous AlGaN/AlN quantum dot SLs in a NW geometry.

In this work, we describe the growth and characterization of N-polar $Al_xGa_{1-x}N$/AlN (x=0, 0.1) quantum dot SLs grown as extensions on GaN NWs and designed for their application in electron-pumped UV sources. The NWs are grown using plasma-assisted MBE on n-type Si(111) wafers using a low temperature AlN nucleation layer. Growth conditions are tuned to obtain a high density of non-coalesced GaN NWs. On top of them, the $Al_xGa_{1-x}N$/AlN active region is 400 nm long (88 periods of quantum dots). Such structures present single-line spectral emission with IQE that can reach 63%.

2. Results and discussion

Self-assembled N-polar GaN NWs were synthesized using plasma-assisted molecular beam epitaxy (PAMBE) on n-type Si(111) substrates using a low-temperature AlN nucleation layer, as described elsewhere [24,25]. To improve the height uniformity [26], the growth began with a long (~900 nm) NW base with a diameter of 30-50 nm, grown under N-rich conditions (Ga/N flux ratio: $\Phi_{Ga}/\Phi_N = 0.25$) at a substrate temperature $T_S = 810°C$ and at a growth rate $v_G = 290$ nm/h. The choice of growth conditions is based on the study described in **figure 1**. From these bird's eye and top-view scanning electron microscopy (SEM) images, we observe that increasing the substrate temperature from 770°C to 810°C results in a reduction of the NW density, at the price of a slight decrease of the growth rate due to the enhancement of GaN decomposition. However, at 825°C the decomposition rate is too high, and the NW height becomes highly inhomogeneous.

The growth of the GaN base was followed by the deposition of a 400-nm-long $Al_xGa_{1-x}N$/AlN (x = 0, 0.10) SL, i.e. 88 periods of quantum dots. The $Al_xGa_{1-x}N$ dots were grown using the same Ga flux as for the NW base, and adding an Al flux $\Phi_{Al} = x/v_G$, where x is the targeted Al mole fraction. The AlN sections were grown at the stoichiometry ($\Phi_{Al}/\Phi_N = 1$). The whole SL was synthesized without any growth interruption. To adjust the spectral response, we varied

the dot/barrier thickness ratio and the Al content in the dots, maintaining the number of periods (88) and the period length (4.5 nm) constant. The values of Al mole fraction in the dots given in this manuscript are nominal values. From the position of the (0002) reflection of the quantum dot SL in x-ray diffraction studies we estimate that the error bar in the composition is in the range of ± 2%. The Al mole fraction in the $Al_xGa_{1-x}N$ dots was kept intentionally low, around x = 0.1, to prevent deformations of the nanowire morphology and reduce the effects of alloy inhomogeneities, observed for $x \geq 0.3$ [18]. The nominal characteristics of the samples presented here are listed in **table 1**.

Figures 2(a) and (b) present typical (a) cross-section and (b) top-view SEM images of an as-grown sample of GaN NWs containing an $Al_xGa_{1-x}N$/AlN SL, e.g. the image corresponds to a sample with 88 periods of $Al_{0.1}Ga_{0.9}N$ / AlN (sample S4). The NWs are detached from each other, but highly packed. Top view images point to a NW density of $6\text{-}8\times10^9$ cm^{-3}. The NW diameter is in the range of 30-50 nm at the base, increasing to 50-70 nm in the top region due to the enhancement of lateral growth when depositing AlN [27,28].

The as-grown NW ensemble was characterized using XRD in order to validate the periodicity of the structure, with the results illustrated in **Figure 2(c)**. These measurements provide average information over a surface of several millimeters squared, and are hence sensitive to the dispersion of tilts and twists in the NW ensemble. Several satellites of the (0002) reflection of the SL are resolved, which confirms the thickness uniformity along the growth axis and the reproducibility of the period length from sample to sample (period = 4.3±0.2 nm). It should be noticed that the (0002) reflection of GaN originated by the NW base is not located at the angular position of relaxed GaN ($2\theta = 34.57°$), but at slightly larger angles.

To get highly resolved information on the NW structure, the NWs were dispersed on holey carbon membranes for scanning transmission electron microscopy (STEM) observations. **Figure 3(a-b)** presents high-angle annular dark field (HAADF) STEM images of a GaN/AlN (1.5 nm / 3.0 nm) SL (88 periods) on a GaN NW (sample S1). The dots display regular thickness

along the NW, and the whole GaN/AlN SL is enveloped by an AlN shell. **Figure 3(c)** shows a high magnification HAADF-STEM view of an $Al_{0.1}Ga_{0.9}N$/AlN (0.65 nm / 3.85 nm) SL (sample S5), which confirms the nominal layer thicknesses and the homogeneity of the structure. In both samples, we observe a decrease of the thickness of the AlN shell along the growth axis, which is more important in the sample with higher Al content in the SL. This is consistent with the fact that the AlN shell forms as a result of the low mobility and of the Al atoms impinging on the NW sidewalls. From STEM analysis of various NWs, the thickness of the shell is estimated to be only 1-2% of the axial AlN thickness. The presence of the AlN shell imposes a uniaxial compressive stress to the GaN base, which justifies the shift of the GaN (0002) XRD reflection as observed in **Figure 2(c)**.

Optical characterization by cathodoluminescence (CL) at room temperature, with an electron acceleration voltage V_A = 5 kV, is presented in **Figure 4(a)**. The emission blue shifts when we decrease the dot height and increase their Al content. A spectral shift from 340 nm to 260 nm is demonstrated while maintaining approximately the same spectral linewidth. The acceleration voltage (V_A) determines the penetration depth of the electrons in the structure, which depends mostly on the material density [6]. The thickness of the SL was initially decided by assuming that the sample behaves similar to a planar structure with the same geometry along the growth axis. However, in a NW ensemble, the average material density is smaller, and there is a risk of electron channeling when the direction of impinging electrons is perpendicular to the silicon substrate. To assess the relevance of these phenomena, we have studied the variation of the CL spectra as a function of V_A, as shown in **Figure 4(b)**. If the emission spectra are normalized to their maximum, the emission from the GaN base becomes visible only for V_A > 5 kV. This implies that the NW ensemble is compact enough to prevent important deviations of their behavior with respect to planar structures.

Finally, we have assessed the IQE of the samples by analyzing the variation of their emission, either photoluminescence (PL) or CL, as a function of temperature. As an example,

Figure 5(a) displays the evolution of the PL spectrum as a function of temperature for a sample containing an $Al_{0.1}Ga_{0.9}N$/AlN (0.75 nm / 3.75 nm) SL (sample S4). **Figure 5(b)** depicts the integrated luminescence intensity from S4 as a function of the inverse temperature measured both by PL and CL, showing that there is no significant difference between the two measuring techniques. The variation of the integrated PL intensity from S1 with temperature is also presented.

The IQE is often estimated as the ratio of the integrated luminescence intensity at room temperature and at low temperature: IQE ≈ I(300 K) / I(0 K). However, it should be kept in mind that this expression assumes that I(0 K) is not affected by non-radiative processes. Overestimation of the IQE can happen if non-radiative recombination paths are active at low temperature, but also if the pumping intensity is high enough to saturate non-radiative recombination paths at high temperature. The measured IQE is also higher under pulsed excitation, due to the difference in the behavior of radiative and non-radiative recombination with respect to time. To get a reliable measurement, our PL experiments were performed under continuous wave excitation, using very low power densities (10 µW pumping power focused on a spot with a diameter around 100 µm). The fact that the luminescence intensity is almost constant up to 50 K is an indication that non-radiative recombination is negligible at low temperature (≈ 6 K). Therefore, we can assume that the expression IQE ≈ I(300 K) / I(≈ 6 K) is valid in our case. Following this reasoning, the IQE values of the samples under study are summarized in **table 1**. In particular, from **figure 5(b)** we can extract an IQE ≈ 44% for sample S4, emitting at 286 nm. This value increases up to IQE ≈ 63% for S1, emitting at 340 nm, and it decreases to ≈ 22% for S5, emitting at 258 nm.

It is important to keep in mind that the IQE values reported above describe the intrinsic material properties of the structures, i.e. they refer to the ratio between radiative recombination and total recombination when the perturbation introduced by the excitation source is minimum

(continuous wave excitation, power density around 0.00013 kW/cm^2). The most common values reported as IQE in the literature for AlGaN LEDs are measured under pulsed excitation [29–38], using power densities in the range of 5-1000 kW/cm^2 [29–32,34,35]. This leads to photogenerated carrier densities higher than the doping level of the original structure, to emulate the carrier density under operation conditions. In such a situation, nonradiative recombination paths are partially saturated, so that the obtained IQE is often significantly higher than the low-injection value, and depends on the excitation power density [29–32,35,39].

In the case of high injection, the calculation of the IQE must take into account the drop of PL efficiency at low temperature due to the high-power excitation [35]:

$$IQE(P) = \frac{I(300\ \mathrm{K},P)}{I(0\ \mathrm{K},P)} \times \frac{I(0\ \mathrm{K},P)}{I(0\ \mathrm{K},low\ injection)} \quad (1)$$

where $I(T,P)$ is the integrated PL intensity as a function of temperature and excitation power (P). We have measured the PL of the NWs as a function of the excitation power using a pulsed Nd-YAG laser (266 nm, 2 ns pulses with a repetition rate of 8 kHz). Measurements were performed at 6 K and at 300 K, and the room-temperature IQE was calculated using equation 1. The results for samples S1 and S2, presented in the inset of **figure 5(b)**, show that the NW samples are stable enough to stand pulsed operation at high power densities up to around 50 kW/cm^2 without degradation of the IQE. Note that in an electron-pumped UV lamp, using an acceleration voltage of 5 kV and an injection current of 1 mA to irradiate a spot with a diameter of 1 mm, the excitation density would be below 1 kW/cm^2

3. Conclusion

In summary, we have demonstrated the synthesis and characterization of $Al_xGa_{1-x}N$/AlN (x = 0, 0.1) quantum dot SLs on GaN NWs designed for application in electron-pumped UV sources. The $Al_xGa_{1-x}N$/AlN active region is 400 nm long (88 periods of quantum dots), long enough to collect the electron-hole pairs generated by an electron beam with an acceleration voltage

≤ 5 kV. The NWs are grown using plasma-assisted MBE on n-type Si(111) wafers using a low temperature AlN nucleation layer. To adjust the spectral response, we have varied the dot/barrier thickness ratio and the Al content in the dots. By growing the $Al_xGa_{1-x}N$ quantum dots under N-rich conditions and the AlN barriers at the stoichiometry, we obtain SLs with a regular periodicity along the whole active region. In all the cases, the room temperature emission is dominated by a single spectral line that can be tuned from 340 nm (IQE > 60%), to 286 nm (IQE = 44 %) and 258 nm (IQE = 22%).

In this manuscript, we have focused on the assessment of these nanostructures in terms of internal quantum efficiency and stability under electron pumping. The estimation of the wall plug efficiency should consider the complete system, including carrier injection losses and light extraction efficiency. To reduce carrier injection losses, cold cathodes with efficiencies close to unity are nowadays available [40,41] , and the design of the semiconductor structure should follow the advices discussed in this paper (particularly the superlattice total length and high nanowire density), so that the free carriers generated by impact ionization recombine within the active region of the device. Regarding light extraction, the nanowire geometry should result in improved performance in comparison with planar layers [15], but the effect of the substrate and the GaN stem should be quantified. If relevant, the potential advantage of detaching the nanowire ensemble from the silicon substrate should be explored [42].

4. Experimental Section

X-ray diffraction (XRD) measurements where performed in a Rigaku SmartLab x-ray diffractometer using a 4 bounce Ge(220) monochromator and a long plate collimator of 0.228° for the secondary optics.

The morphology of the as-grown NW ensemble was studied by field-emission scanning electron microscopy (SEM) using a Zeiss Ultra 55 microscope.

Detailed structural studies were conducted using high-resolution transmission electron microscopy (HR-TEM) and high-angle annular dark-field scanning transmission electron microscopy (HAADF-STEM) performed on a probe-corrected FEI Titan Themis microscope operated at 200 kV.

Cathodoluminescence (CL) experiments were performed using a field-emission SEM FEI Inspect F50 equipped with a low-temperature Gatan stage to cool the sample down to 6 K, and with an IHR550 spectrometer.

Photoluminescence (PL) spectra were obtained by excitation with a frequency-doubled continuous-wave solid-state laser (λ = 244 nm), with an optical power of ≈ 10 µW focused on a spot with a diameter of ≈ 100 µm. Additionally, PL measurements under pulsed excitation were performed using a Nd-YAG laser (266 nm, 2 ns pulses with a repetition rate of 8 kHz) focused on a spot with a diameter of ≈ 100 µm. In both cases, the sample was mounted on a cold-finger cryostat, and its emission was collected by a Jobin Yvon HR460 monochromator equipped with a UV-enhanced charge-coupled device (CCD) camera.

Acknowledgements

This work is supported by the French National Research Agency (ANR) via the UVLASE program (ANR-18-CE24-0014), and by the Auvergne-Rhône-Alpes region (grant PEAPLE). This project has also received funding from the European Research Council under the European Union's H2020 Research and Innovation programme via the e-See project (grant #758385). We also acknowledge technical support from F. Jourdan, Y. Curé and Y. Genuist. We benefited from the access to the technological platform NanoCarac of CEA-Minatech Grenoble in collaboration with the IRIG-LEMMA group.

Received: ((will be filled in by the editorial staff))
Revised: ((will be filled in by the editorial staff))
Published online: ((will be filled in by the editorial staff))

References

[1] M. A. Würtele, T. Kolbe, M. Lipsz, A. Külberg, M. Weyers, M. Kneissl, M. Jekel, *Water Research* **2011**, *45*, 1481.

[2] R. Collazo, S. Mita, J. Xie, A. Rice, J. Tweedie, R. Dalmau, Z. Sitar, *physica status solidi (c)* **2011**, *8*, 2031.

[3] M. L. Nakarmi, K. H. Kim, M. Khizar, Z. Y. Fan, J. Y. Lin, H. X. Jiang, *Appl. Phys. Lett.* **2005**, *86*, 092108.

[4] Y. Nagasawa, A. Hirano, *Applied Sciences* **2018**, *8*, 1264.

[5] Herbert J. Reich, *Principles of Electron Tubes*, Literary Licensing, LLC, **2013**.

[6] H. J. Leamy, *Journal of Applied Physics* **1982**, *53*, R51.

[7] T. Oto, R. G. Banal, K. Kataoka, M. Funato, Y. Kawakami, *Nature Photonics* **2010**, *4*, 767.

[8] T. Matsumoto, S. Iwayama, T. Saito, Y. Kawakami, F. Kubo, H. Amano, *Optics Express* **2012**, *20*, 24320.

[9] Y. Shimahara, H. Miyake, K. Hiramatsu, F. Fukuyo, T. Okada, H. Takaoka, H. Yoshida, *Applied Physics Express* **2011**, *4*, 042103.

[10] S. V. Ivanov, V. N. Jmerik, D. V. Nechaev, V. I. Kozlovsky, M. D. Tiberi, *physica status solidi (a)* **2015**, *212*, 1011.

[11] Y. Wang, X. Rong, S. Ivanov, V. Jmerik, Z. Chen, H. Wang, T. Wang, P. Wang, P. Jin, Y. Chen, V. Kozlovsky, D. Sviridov, M. Zverev, E. Zhdanova, N. Gamov, V. Studenov, H. Miyake, H. Li, S. Guo, X. Yang, F. Xu, T. Yu, Z. Qin, W. Ge, B. Shen, X. Wang, *Advanced Optical Materials* **2019**, *7*, 1801763.

[12] H. Sun, J. Woodward, J. Yin, A. Moldawer, E. F. Pecora, A. Yu. Nikiforov, L. Dal Negro, R. Paiella, K. Ludwig, D. J. Smith, T. D. Moustakas, *Journal of Vacuum Science*

& Technology B, Nanotechnology and Microelectronics: Materials, Processing, Measurement, and Phenomena **2013**, *31*, 03C117.

[13] T. Hayashi, Y. Kawase, N. Nagata, T. Senga, S. Iwayama, M. Iwaya, T. Takeuchi, S. Kamiyama, I. Akasaki, T. Matsumoto, *Scientific Reports* **2017**, *7*, 2944.

[14] T. Wunderer, J. Jeschke, Z. Yang, M. Teepe, M. Batres, B. Vancil, N. Johnson, *IEEE Photonics Technology Letters* **2017**, *29*, 1344.

[15] M. Djavid, Z. Mi, *Appl. Phys. Lett.* **2016**, *108*, 051102.

[16] M. Beeler, C. B. Lim, P. Hille, J. Bleuse, J. Schörmann, M. de la Mata, J. Arbiol, M. Eickhoff, E. Monroy, *Phys. Rev. B* **2015**, *91*, 205440.

[17] L. F. Zagonel, S. Mazzucco, M. Tencé, K. March, R. Bernard, B. Laslier, G. Jacopin, M. Tchernycheva, L. Rigutti, F. H. Julien, R. Songmuang, M. Kociak, *Nano Lett.* **2011**, *11*, 568.

[18] C. Himwas, M. den Hertog, L. S. Dang, E. Monroy, R. Songmuang, *Applied Physics Letters* **2014**, *105*, 241908.

[19] L. Rigutti, J. Teubert, G. Jacopin, F. Fortuna, M. Tchernycheva, A. De Luna Bugallo, F. H. Julien, F. Furtmayr, M. Stutzmann, M. Eickhoff, *Physical Review B* **2010**, *82*, 235308.

[20] F. Furtmayr, J. Teubert, P. Becker, S. Conesa-Boj, J. R. Morante, A. Chernikov, S. Schäfer, S. Chatterjee, J. Arbiol, M. Eickhoff, *Physical Review B* **2011**, *84*, 205303.

[21] S. D. Carnevale, J. Yang, P. J. Phillips, M. J. Mills, R. C. Myers, *Nano Lett.* **2011**, *11*, 866.

[22] C. Rivera, U. Jahn, T. Flissikowski, J. Pau, E. Muñoz, H. T. Grahn, *Physical Review B* **2007**, *75*, 045316.

[23] L. F. Zagonel, L. Rigutti, M. Tchernycheva, G. Jacopin, R. Songmuang, M. Kociak, *Nanotechnology* **2012**, *23*, 455205.

[24] A. Ajay, C. B. Lim, D. A. Browne, J. Polaczynski, E. Bellet-Amalric, M. I. den Hertog, E. Monroy, *physica status solidi (b)* **2017**, *254*, 1600734.

[25] M. Musolino, A. Tahraoui, S. Fernández-Garrido, O. Brandt, A. Trampert, L. Geelhaar, H. Riechert, *Nanotechnology* **2015**, *26*, 085605.

[26] K. K. Sabelfeld, V. M. Kaganer, F. Limbach, P. Dogan, O. Brandt, L. Geelhaar, H. Riechert, *Appl. Phys. Lett.* **2013**, *103*, 133105.

[27] R. Songmuang, T. Ben, B. Daudin, D. González, E. Monroy, *Nanotechnology* **2010**, *21*, 295605.

[28] R. Calarco, R. J. Meijers, R. K. Debnath, T. Stoica, E. Sutter, Hans. Lüth, *Nano Lett.* **2007**, *7*, 2248.

[29] M. Shatalov, J. Yang, W. Sun, R. Kennedy, R. Gaska, K. Liu, M. Shur, G. Tamulaitis, *Journal of Applied Physics* **2009**, *105*, 073103.

[30] K. Ban, J. Yamamoto, K. Takeda, K. Ide, M. Iwaya, T. Takeuchi, S. Kamiyama, I. Akasaki, H. Amano, *Appl. Phys. Express* **2011**, *4*, 052101.

[31] Z. Bryan, I. Bryan, J. Xie, S. Mita, Z. Sitar, R. Collazo, *Appl. Phys. Lett.* **2015**, *106*, 142107.

[32] H. Murotani, D. Akase, K. Anai, Y. Yamada, H. Miyake, K. Hiramatsu, *Appl. Phys. Lett.* **2012**, *101*, 042110.

[33] Y. Liao, C. Thomidis, C. Kao, T. D. Moustakas, *Appl. Phys. Lett.* **2011**, *98*, 081110.

[34] R. G. Banal, M. Funato, Y. Kawakami, *Appl. Phys. Lett.* **2011**, *99*, 011902.

[35] J. Mickevičius, G. Tamulaitis, M. Shur, M. Shatalov, J. Yang, R. Gaska, *Appl. Phys. Lett.* **2012**, *101*, 211902.

[36] A. Bhattacharyya, T. D. Moustakas, L. Zhou, David. J. Smith, W. Hug, *Appl. Phys. Lett.* **2009**, *94*, 181907.

[37] G.-D. Hao, N. Tamari, T. Obata, T. Kinoshita, S. Inoue, *Opt. Express* **2017**, *25*, A639.

[38] P. Dong, J. Yan, Y. Zhang, J. Wang, J. Zeng, C. Geng, P. Cong, L. Sun, T. Wei, L. Zhao, Q. Yan, C. He, Z. Qin, J. Li, *Journal of Crystal Growth* **2014**, *395*, 9.

[39] C. Frankerl, M. P. Hoffmann, F. Nippert, H. Wang, C. Brandl, N. Tillner, H.-J. Lugauer, R. Zeisel, A. Hoffmann, M. J. Davies, *Journal of Applied Physics* **2019**, *126*, 075703.

[40] Y. Cheng, O. Zhou, *Comptes Rendus Physique* **2003**, *4*, 1021.

[41] W. A. de Heer, A. Ch telain, D. Ugarte, *Science* **1995**, *270*, 1179.

[42] K. E. Plass, M. A. Filler, J. M. Spurgeon, B. M. Kayes, S. Maldonado, B. S. Brunschwig, H. A. Atwater, N. S. Lewis, *Adv. Mater.* **2009**, *21*, 325.

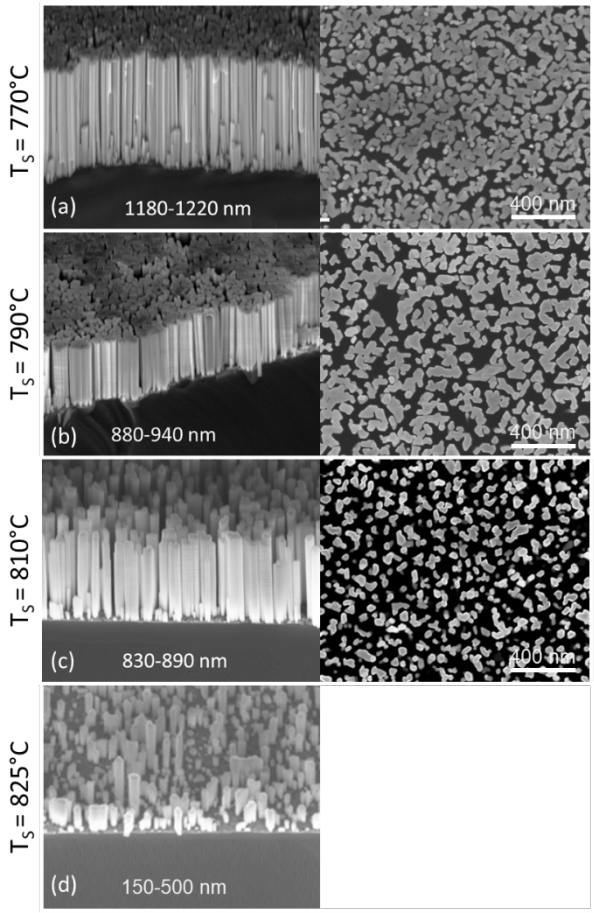

Figure 1. SEM images (bird's eye on the left and top view on the right side) of GaN NW samples grown at various substrates temperatures: (a) 770°C, (b) 790°C, (c) 810°C, and 825 °C. The NW height is indicated as a legend in the bird's eye figure. All the samples grew for 3 hours with a flux ratio $\Phi_{Ga}/\Phi_N = 0.25$.

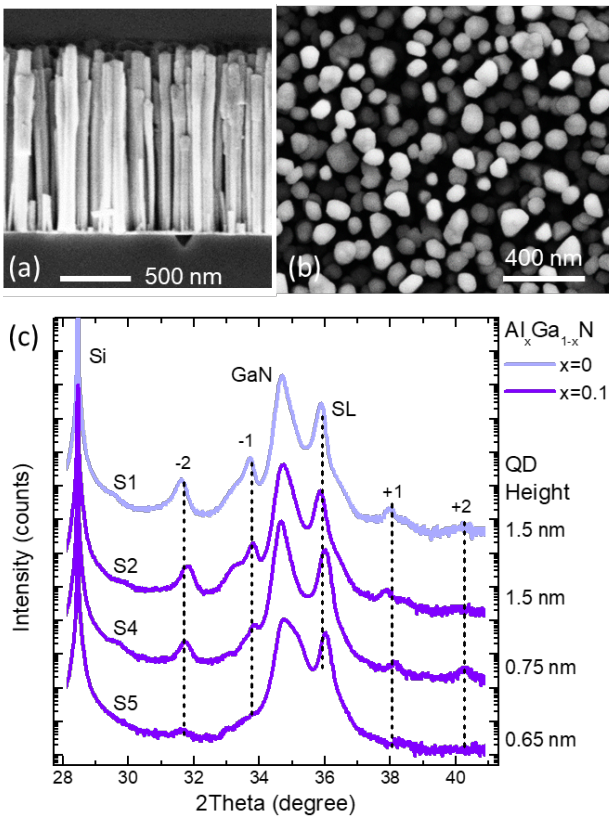

Figure 2. (a) Cross-section and (b) top-view SEM images of a sample containing GaN NWs with a superlattice (SL) consisting of 88 periods of $Al_{0.1}Ga_{0.9}N$/AlN (S4). (c) XRD θ–2θ scans of the (0002) reflection of GaN NWs containing an 88-period $Al_xGa_{1-x}N$/AlN quantum dot SL. The nominal Al concentration is color-coded and the height of the quantum dots (QD) is indicated on the right side of the figure. The diffractograms are vertically shifted for clarity.

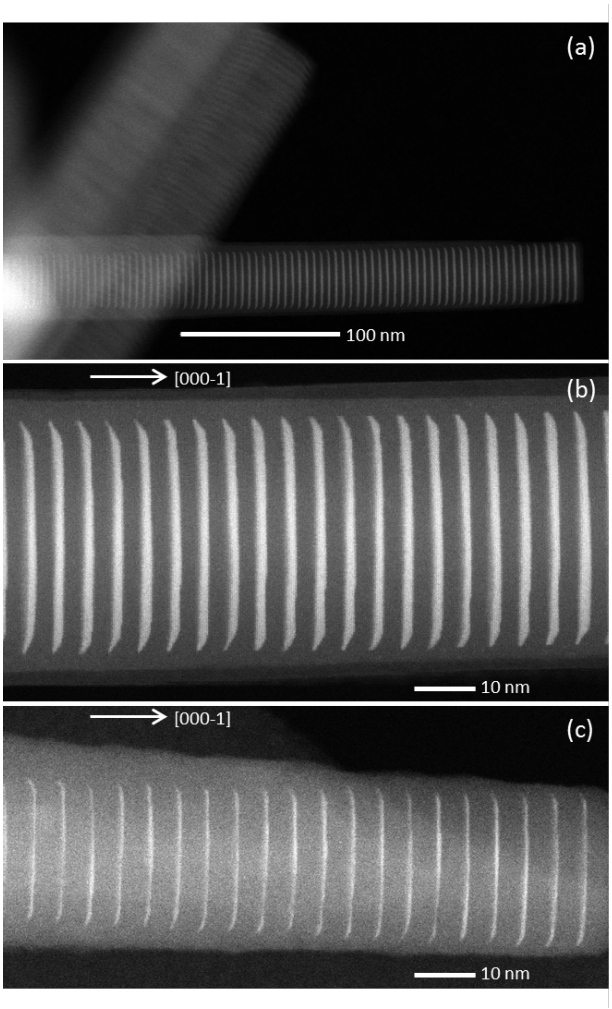

Figure 3. (a) HAADF-STEM image of dispersed NWs containing 88 periods of GaN/AlN (1.5 nm/3.0 nm). The bright contrast is GaN and the darker contrast represents AlN. Note that in HAADF-STEM the contrast of the image provides chemical information. (b) High-magnification HAADF-STEM image of a NW containing 88 periods of GaN/AlN (S1). (c) High-magnification HAADF-STEM image of a NW containing 88 periods of $Al_{0.1}Ga_{0.9}N$/AlN (S5).

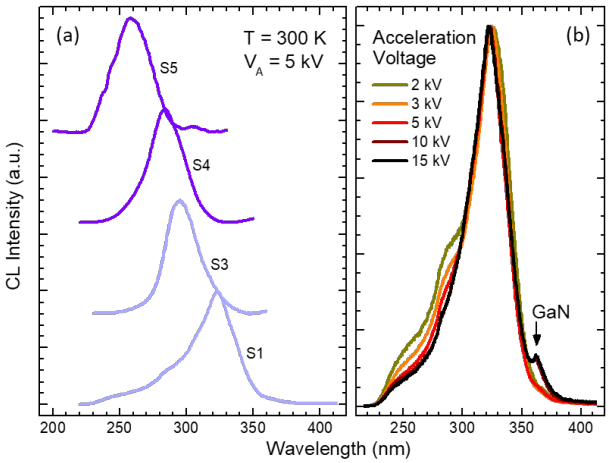

Figure 4. Room-temperature CL measurements of NWs containing an 88-period AlGaN/AlN quantum dot SL. (a) Measurements performed at an acceleration voltage V_A = 5 kV of samples with the following SL structures: S1: 1.5 nm GaN / 3.0 nm AlN, S3: 0.75 nm GaN / 3.75 nm AlN, S4: 0.75 nm $Al_{0.1}Ga_{0.9}N$ / 3.75 nm AlN, S5: 0.65 nm $Al_{0.1}Ga_{0.9}N$ / 3.85 nm AlN. (b) Normalized CL spectra of the S4 structure as a function of the accelerating voltage. The emission from the GaN stem of the NWs is only resolved for V_A > 5 kV.

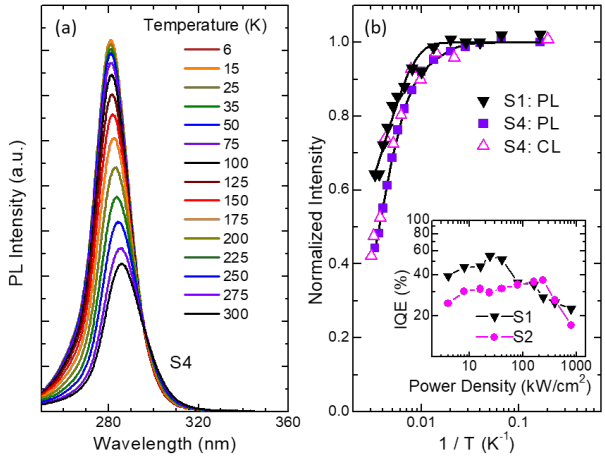

Figure 5. (a) Variation of the PL spectra as a function of temperature (sample S3: 0.75 nm $Al_{0.1}Ga_{0.9}N$ / 3.75 nm AlN). (b) Variation of the integrated PL intensity of S1 and S4, and the integrated CL intensity of S4 as a function of the inverse temperature, normalized to their value at low temperature. The solid lines are fits to $1/[1 + A \exp(-E_a/(kT))]$, where E_a is a thermal activation energy, kT is the thermal energy, and A is a fitting constant. For S1, E_a = 38±5 meV and A = 2.3±0.5. For S4, E_a = 48±4 meV and A = 7±2. Inset: Variation of the IQE as a function of the excitation power density, measured with a pulsed laser.

Table 1. Nominal characteristics of the samples under study: AlN barrier thickness (t_B), GaN dot height (t_{QD}), Al mole fraction in the dots (x). Peak emission wavelength at room temperature (λ_{RT}), full width at half maximum of the emission at room temperature ($FWHM_{RT}$) and IQE.

Sample	t_B (nm)	t_{QD} (nm)	x	λ_{RT} (nm)	$FWHM_{RT}$ (nm)	IQE (%)
S1	3.0	1.5	0	340	31	63
S2	3.0	1.5	0.1	335	29	42
S3	3.75	0.75	0	296	22	48
S4	3.75	0.75	0.1	286	16	44
S5	3.85	0.65	0.1	258	34	22

ToC entry:

This paper describes the fabrication of AlGaN/AlN quantum dot superlattices on GaN nanowires for application in electron-pumped UV sources. The active region is designed to collect the carriers generated by an electron beam with an acceleration voltage of 5 kV. The emission is tuned in the 340 to 258 nm range by varying the dot/barrier thickness ratio and the Al content in the dots.

Keywords: ultraviolet, nanowires, AlGaN, quantum dot, lamp

I. Dimkou, A. Harikumar, A. Ajay, F. Donatini, E. Bellet-Amalric, A. Grenier, M. I. den Hertog, S. T. Purcell, and E. Monroy*

Design of AlGaN/AlN dot-in-a-wire heterostructures for electron-pumped UV emitters

ToC figure: